

# Magnetic dipole and Gamow-Teller modes: quenching, fine structure and astrophysical implications

**A Richter**

Institut für Kernphysik, Technische Universität Darmstadt, 64289 Darmstadt, Germany

E-mail: richter@ikp.tu-darmstadt.de

**Abstract.** The magnetic dipole (M1) and Gamow-Teller (GT) response are prime examples to illustrate the importance of configuration mixing for an understanding of elementary excitation modes of the nucleus. Starting from the "classical" problem of quenching – whose proper description is still beyond the capabilities of microscopic models after all those years – I want to address some current developments of the field. Mandatory for the progress are high-resolution data from electron and hadron scattering and charge-exchange reactions.

In medium-mass fp-shell nuclei, the detailed knowledge of the M1 and GT strength distribution provides a stringent test of state-of-the-art shell-model calculations, validating their applicability in astrophysical network calculations. As an example, it is demonstrated that high-precision M1 data on  $N = 28$  isotones from electron scattering at Darmstadt permit the extraction of neutral-current neutrino-nucleus scattering cross sections important for supernova dynamics and nucleosynthesis.

Fine structure of the GT mode is not only observed in light and medium-mass nuclei, but also in the GT resonance observed in a heavy nucleus like  $^{90}\text{Nb}$  studied in the  $^{90}\text{Zr}(^3\text{He},t)$  reaction at Osaka with a resolution  $\Delta E \simeq 50$  keV (FWHM). Novel methods, based on wavelet transforms, to extract scales characterizing the fine structure are presented. This in turn permits an interpretation of the physics underlying the phenomenon. These methods can also be used to extract spin- and parity-resolved level densities in a nearly model-independent way, again important to test models used in various astrophysical scenarios.

As a final example, the influence of configuration mixing on the GT strength distribution at low energies is investigated for the heavy odd-odd nuclei  $^{138}\text{La}$  and  $^{180}\text{Ta}$ . The nucleosynthesis of these exotic nuclides, amongst the rarest in nature, is a long-standing problem. A likely source are charged-current neutrino-nucleus reactions which would be dominated by the GT response. However, the main GT resonance lies above the particle threshold and, therefore, does not contribute. Recent measurements of the GT strength distributions in  $^{138}\text{La}$  and  $^{180}\text{Ta}$  below the particle threshold and their astrophysical implications are discussed.

## 1. Introduction

In this symposium on the occasion of the 50th anniversary of the Arima-Horie theory of configuration mixing [1] it is certainly appropriate to first ask the question why is it important to study the magnetic dipole (M1) response in nuclei and what is known about this response. Very briefly, if ( $i$ ) static magnetic moments  $\vec{\mu}_j$ , i.e. *diagonal* matrix elements of the M1 operator and their orbital and spin parts  $\vec{\mu}_l$  and  $\vec{\mu}_s$ , respectively, deviate from the lowest order shell model expectations usually mesonic currents and configuration mixing effects are made

responsible for this [2]. The effect of first order configuration mixing considered by Arima and Horie in their seminal paper [1] in 1954 is now treated in large-scale shell model calculations (often by introducing an effective operator  $\vec{\mu}_{eff}$ ). But additional information on the nuclear magnetic dipole response is obtained through the study of (ii) magnetic dipole transitions, which determine the *off-diagonal* matrix elements of the transition operator. Since the M1 operator is primarily of single particle nature, individual neutron and proton excitations might be investigated separately, but also their possible interference reflected in isoscalar vs. isovector excitations and in the interplay between spin and orbital magnetization. The prime example of an almost pure orbital excitation is the scissors mode [3, 4] where in deformed nuclei protons are set into rotation vs. neutrons in a scissors-like fashion. Since the M1 operator contains both an orbital and a spin part, but the Gamow-Teller operator only a spin part, different probes like (iii)  $\beta$  decay, (p,p') (p,n), (n,p) (d,<sup>2</sup>He), (<sup>3</sup>He,t), (t,<sup>3</sup>He) ... reactions should help to disentangle this interplay.

The existing substantial body of experimental transition rates points to a quenching of the spin-isospin strength  $\vec{\sigma}\vec{\tau}$  by about 50% with respect to the usual single particle (s.p.) estimates. A mechanism similar to 2nd order configuration mixing (2p-1h) of 2p-2h configurations is mostly responsible for it [5], or expressed somewhat differently: s.p. transitions are influenced by an accompanying polarization cloud of p-h excitations. The highly excited ones of those are induced by the tensor force – the mechanism called  $n\hbar\omega$  core polarization. For all what we know now the external magnetic dipole field exciting the  $\vec{\sigma}\vec{\tau}$  transitions couples to a very large extent solely to nuclear degrees of freedom, i.e. effects of coupling of the nucleon to the  $\Delta(1232)$  isobar,  $(\Delta - N^{-1})$  transitions are small. Finally, (iv)  $\vec{\sigma}\vec{\tau}$  transitions have increasing importance in astrophysics.

These salient features (i) to (iv) have been illustrated much more extensively in the oral presentation of this talk than it is possible in the very limited space allocated for its write up. The interested reader is thus either referred to the listed published work or to the ppt presentation available [6].

## 2. Quenching of M1 and GT strength

The M1 response is a fundamental low-energy mode of the nucleus. It can be well explored by means of inelastic electron and photon scattering. Such transitions are mediated by the operator

$$O(M1) = \sqrt{\frac{3}{4\pi}} \sum_k [g_l(k)l(k) + g_s(k)s(k)] \mu_N \quad (1)$$

where  $\mathbf{l}$  and  $\mathbf{s}$  are the orbital and spin angular momentum operators, and the sum runs over all nucleons. The orbital and spin gyromagnetic factors are given by  $g_l = 1$ ,  $g_s = 5.586$  for protons and  $g_l = 0$ ,  $g_s = -3.826$  for neutrons;  $\mu_N$  is the nuclear magneton. Equation (1) can be rewritten in isovector and isoscalar parts. Due to a strong cancellation of the  $g$ -factors in the isoscalar part, the isovector part dominates. The respective isovector M1 operator is given by

$$O(M1)_{iv} = \sqrt{\frac{3}{4\pi}} \sum_k [l(k)t_0(k) + (g_s^p - g_s^n)s(k)t_0(k)] \mu_N. \quad (2)$$

Note that the spin part of the isovector M1 operator is the zero component of the GT operator,

$$O(GT_0) = \sum_k \sigma(k)t_0(k) = \sum_k 2s(k)t_0(k), \quad (3)$$

however, enhanced by the factor  $\sqrt{3/4\pi}(g_s^p - g_s^n)/2 = 2.2993 \mu_N$ .

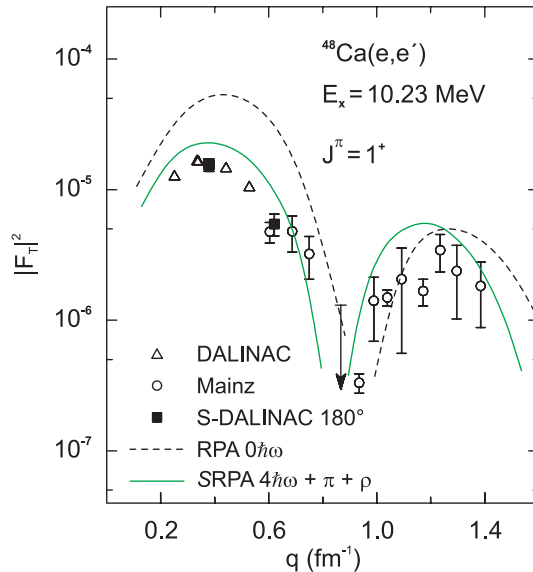


**Figure 1.** Form factor of the  $1f_{7/2} \rightarrow 1f_{5/2}$  M1 transition at  $E_x = 10.23$  meV in  $^{48}\text{Ca}$  from inelastic electron scattering [11] compared to the microscopic calculations of [13].

The GT strength has been shown to be quenched by about 50% in medium-mass to heavy nuclei [7]. The same holds for the M1 response in fp-shell nuclei [8] and  $^{208}\text{Pb}$  [9]. The long-standing question whether this quenching is caused by higher-order configuration mixing or  $(\Delta - N^{-1})$  isobar transitions seems to be answered in favor of the former [10]. Nevertheless, the microscopic description of the quenching phenomenon remains a challenge to nuclear structure theory. The  $(e, e')$  form factor of the famous neutron  $1f_{7/2} \rightarrow 1f_{5/2}$  M1 transition in  $^{48}\text{Ca}$  [11] displayed in Fig. 1 remains *the* test case of microscopic models. The data (including recent results from  $180^\circ$  scattering at the S-DALINAC [12]) are confronted with a  $0\hbar\omega$  RPA calculation which not only grossly overpredicts the M1 strength but also fails to properly describe the momentum transfer dependence. If one includes the 2p-2h coupling (SRPA) plus  $\pi$  and  $\rho$  exchange effects in a very large ( $4\hbar\omega$ ) basis, results are significantly improved but deviations remain. Such a calculation, albeit about 15 years old [13], still roughly represents the limits of what can be done within microscopic models today.

### 3. Neutral-current inelastic neutrino-nucleus scattering and M1 response

Inelastic neutral-current neutrino-nucleus scattering plays an important role in many astrophysical applications, including r-process nucleosynthesis, the synthesis of certain elements like  $^{10,11}\text{B}$  and  $^{19}\text{F}$  during a supernova explosion by the  $\nu$ -process or for the detection of supernova neutrinos. Particular relevance is expected in aspects of supernova physics [14, 15]. Although inelastic neutrino-nucleus scattering is not yet considered in supernova simulations, their importance has been pointed out, in particular for nuclei in the iron ( $A \approx 56$ ) mass range [14].

Except for the ground state transition to the  $J = 1^+$ ,  $T = 1$  state in  $^{12}\text{C}$  at an excitation energy  $E_x = 15.11$  MeV [16], currently no data for inelastic neutrino-nucleus scattering is available. However, for some iron-region nuclei precise data on the magnetic dipole (M1) strength distributions exist. It can be shown that these data supply to a large extent the required information about the nuclear Gamow-Teller (GT) distribution and hence determine the inelastic neutrino-nucleus cross sections for supernova neutrino energies. It is also demonstrated that

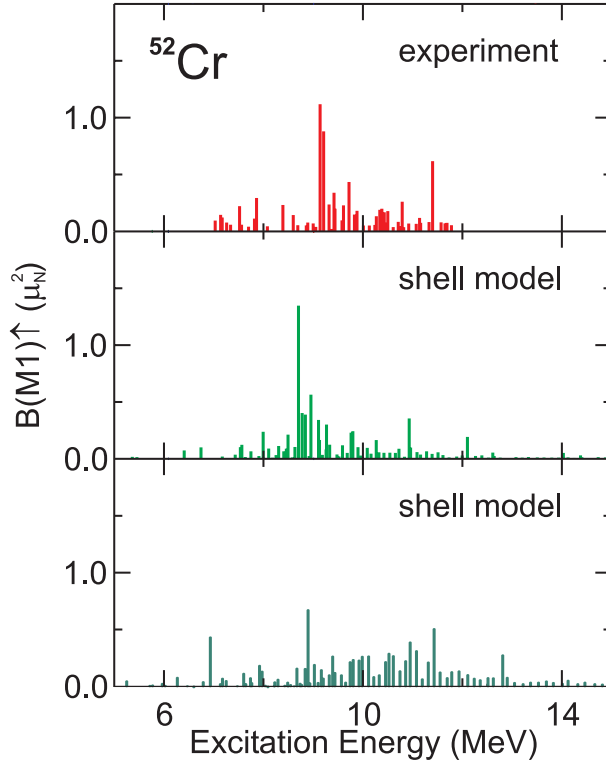


**Figure 2.** Comparison of the experimental M1 strength distribution in  $^{52}\text{Cr}$  from high-resolution  $(e,e')$  experiments [19] (top) with shell-model results using the KB3G [20] (middle) and GXPF1 [21] (bottom) interactions.

large-scale shell-model calculations agree quite well with the precise M1 data, thus validating the use of such models to determine the required cross sections for nuclei where no data exist, or at the finite-temperature conditions in a supernova. Results of this study have been reported in [17].

Examples of spherical  $pf$ -shell nuclei are  $^{50}\text{Ti}$ ,  $^{52}\text{Cr}$  and  $^{54}\text{Fe}$ . As these nuclei have also the advantage that precise M1 response data exist from high-resolution inelastic electron scattering experiments [19] these three nuclei have been chosen for further investigation. The experimental M1 strength distribution of  $^{52}\text{Cr}$  is plotted in the top panel of Fig. 2. The strategy now is to show, in a detailed comparison of data and shell model calculations, that the M1 data indeed represent the desired  $GT_0$  information in a sufficient approximation to transform them into total and differential neutrino-nucleus cross sections. Large-scale shell-model calculations have been performed with the code NATHAN [22] using the KB3G residual interaction [20]. As customary in shell-model calculations, the spin operator was replaced by an effective operator  $s_{eff} = 0.75s$ , where the constant is universal for all  $pf$ -shell nuclei [8]. A decomposition into spin and orbital parts demonstrates that the latter are negligible in these semimagic nuclei. The same holds for isoscalar contributions. The comparison of experimental data and shell-model results presented in Fig. 2 reveals a good correspondence. The essential features of the experimental strength distribution are well described. If another recently suggested effective interaction GXPF1 [21] is used, then the centroid of the spin-flip resonance is shifted somewhat to larger energies but the description is still reasonable.

Inelastic neutrino-nucleus scattering at low energies, where finite momentum transfer corrections can be neglected, is dominated by allowed transitions. The cross section for a

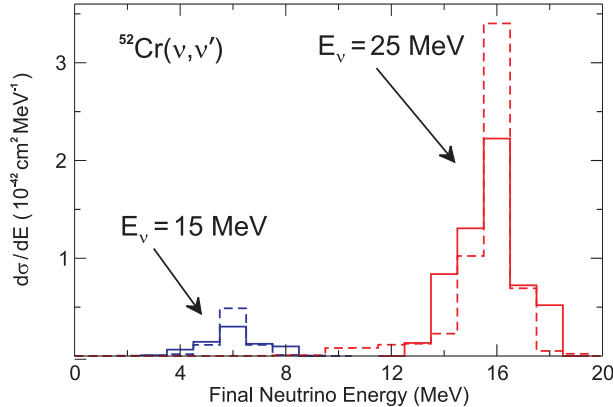


**Figure 3.** Differential inelastic neutrino cross sections for  $^{52}\text{Cr}$  and initial neutrino energies  $E_\nu = 15$  MeV and 25 MeV. The solid histograms are obtained from the M1 data, the dashed ones from shell-model calculations. The final neutrino energies are given by  $E_f = E_\nu - \omega$ .

transition from an initial nuclear state ( $i$ ) to a final state ( $f$ ) is given by [18]

$$\sigma_{i,f}(E_\nu) = \frac{G_F^2 g_A^2}{\pi(2J_i + 1)} (E_\nu - \omega)^2 |\langle f || \sum_k \sigma(k) t(k) || i \rangle|^2, \quad (4)$$

where  $G_F$  and  $g_A$  are the Fermi and axialvector coupling constants, respectively,  $E_\nu$  is the energy of the scattered neutrino and  $\omega$  is the difference between final and initial nuclear energies (for g.s. transitions  $E_x = \omega$ ). The nuclear dependence is contained in the reduced transition probability between the initial and final nuclear states

$$B(GT_0) = \frac{g_A^2}{(2J_i + 1)} |\langle f || \sum_k \sigma(k) t(k) || i \rangle|^2. \quad (5)$$

Supernova simulations require differential neutrino-nucleus cross sections as functions of initial and final neutrino energies, where neutrinos of different flavors are comprised in energy bins of a few MeV [23], i.e. cross sections are averaged over many final nuclear states. Cancelling most of the interference between orbital and spin contributions, the M1 data should represent the desired  $GT_0$  information, simply using the relation  $B(M1) = 3(g_s^p - g_s^n)^2 \mu_N^2 / (16g_A^2 \pi) B(GT_0)$ . Figure 3 shows the differential neutrino cross section for  $^{52}\text{Cr}$  at two representative supernova neutrino energies. The cross sections, obtained from the experimental M1 data and the KB3G shell model result agree quite well, if binned in energy intervals of a resolution (1 MeV or somewhat larger) as required in supernova simulations and it is concluded [17] that modern large-scale shell model results are at a level of precision to indeed permit an inclusion of neutral-current neutrino-nucleus scattering in future supernova models.

#### 4. Fine structure of the GT resonance in the heavy nucleus $^{90}\text{Nb}$

High-resolution studies of the IVGDR [24, 25, 26] and in particular of the ISGQR over a wide mass range [27] provide experimental evidence for fine structure in electric giant resonances. Using a novel method based on wavelet analysis techniques characteristic energy scales can be extracted which were shown to result from the coupling of the initial 1p-1h excitations to 2p-2h states [27]. This important finding immediately raises the question whether fine structure is also found in the Gamow-Teller resonance, i.e. a spin-isospinflip mode. Generally, spin-isospin

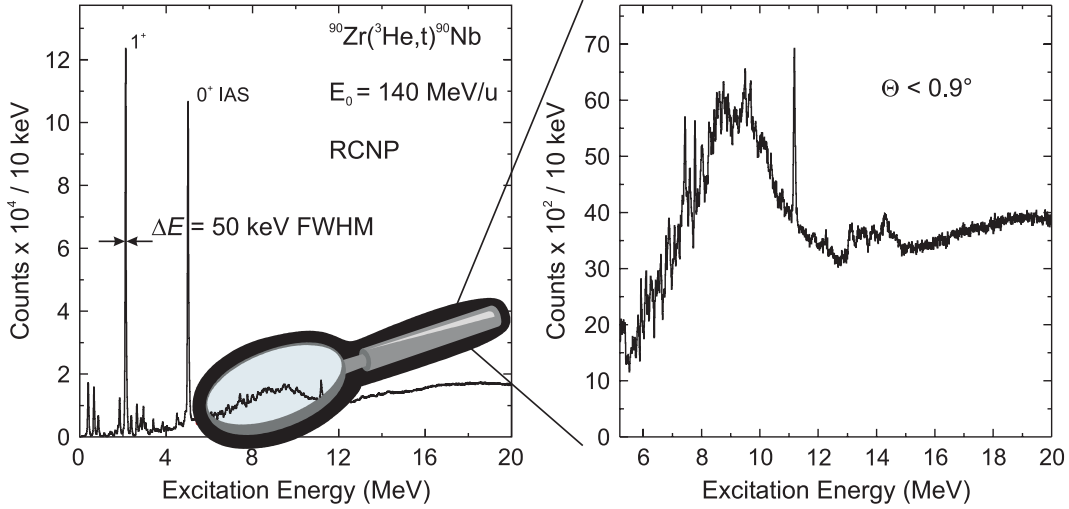


**Figure 4.** Left panel: Spectrum of the  $^{90}\text{Zr}(^3\text{He},t)^{90}\text{Nb}$  reaction at  $E_0 = 140$  MeV/u and  $\Theta < 0.9^\circ$ . The prominent peak at  $E_x \approx 12$  MeV stems from the  $^{12}\text{B}$  g.s. excited in the  $^{12}\text{C}(^3\text{He},t)$  background reaction. Right panel: Zoom on the GT resonance region.

resonances retain more of the single-particle character due to the initial 1p-1h excitations or, in other words, show less collectivity than electric resonances. Indeed, the GT strength in light and medium-mass nuclei exhibits tremendous fine structure if measured with sufficient resolution (see [28]). As an example for a spin-isospin mode in a heavy nucleus, we have performed a study of the  $^{90}\text{Zr}(^3\text{He},t)$  reaction at the RCNP cyclotron in Osaka utilizing the new WS course [29] for the Grand Raiden magnetic spectrometer. It allows experiments with excellent energy resolution approaching 50 keV (FWHM) in heavy nuclei. The l.h.s. of Fig. 4 depicts a spectrum obtained for  $^{90}\text{Nb}$  at an incident energy  $E_0 = 140$  MeV/u and for scattering angles  $\Theta = 0^\circ - 0.9^\circ$ . Under these kinematical conditions, spin-isospin transitions with  $\Delta L = 0$  – i.e. Gamow-Teller (GT) transitions – are selectively enhanced. The r.h.s. of Fig. 4 expands the region of the GT resonance in  $^{90}\text{Nb}$ . The present data beautifully demonstrate the existence of pronounced fine structure. The magnitude of the fluctuations exhibit a remarkable change over the GT resonance and seem to be more damped towards higher excitation energies. Whether this can be purely explained as an effect of the increasing level density is at present an open question.

For an extraction of characteristic scales, a wavelet analysis [30] adopted from signal processing theory is used. By folding the original spectrum  $\sigma(E)$  with a chosen wavelet function  $\Psi$ , coefficients

$$C(E_x, \delta E) = \frac{1}{\sqrt{\delta E}} \int \sigma(E) \Psi \left( \frac{E_x - E}{\delta E} \right) dE \quad (6)$$

are obtained. The parameters (excitation energy  $E_x$  and scale  $\delta E$ ) can be varied continuously or in discrete steps  $\delta E = 2^j$ ,  $E_x = k\delta E$ ,  $j, k = 1, 2, 3, \dots$ , corresponding to continuous (CWT) or discrete (DWT) wavelet transforms, respectively. The results of the continuous wavelet transform are displayed in Fig. 5. The two-dimensional correlation of the absolute values of the wavelet coefficients, Eq. (6), is shown in the lower-right panel. Pronounced maxima extend across the region of the GTR bump at characteristic scale values. The projection on the vertical axis (lower-left panel) allows to extract them more precisely. Scales at 50, 80, 300, 950, and 2600 keV are obtained. The smallest one corresponds to the experimental resolution and the largest one reflects the total width of the resonance (not shown because the scale axis is limited to about 1 MeV for better visibility of the lower scales).

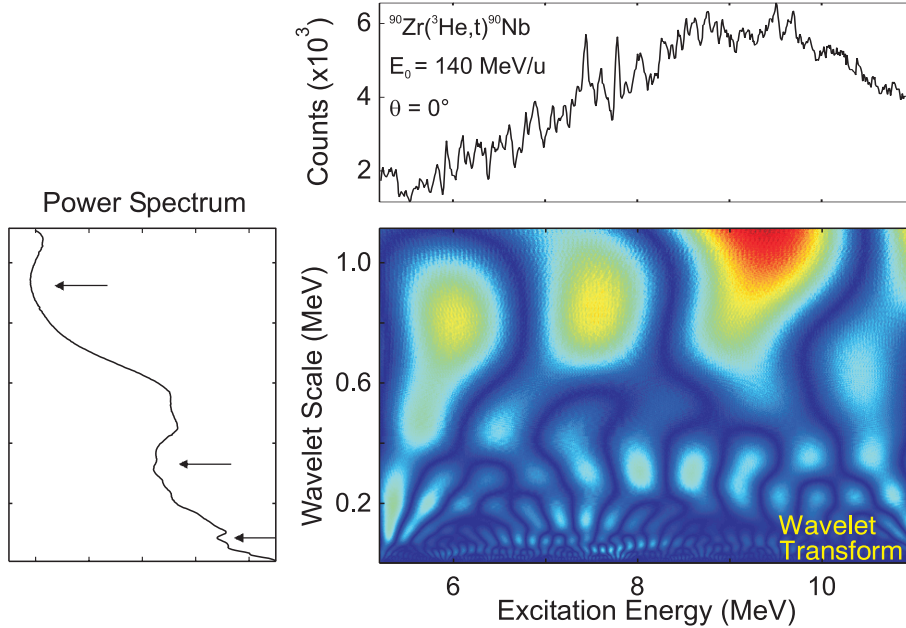


**Figure 5.** Continuous wavelet transform analysis. Upper panel: Spectrum of the  $^{90}\text{Zr}(^3\text{He},t)^{90}\text{Nb}$  reaction. Central panel: Absolute values of the wavelet coefficients, Eq. (6), as a function of excitation energy and scale (right part). Left part: Projection of the wavelet coefficients on the scale axis.

A corresponding analysis of microscopic quasiparticle-phonon model (QPM) results including 2p-2h configurations confirms that the scales arise from the coupling between 1p-1h and 2p-2h states since no scales emerge in a pure 1p-1h calculation. The scales extracted from the QPM results are in fairly good agreement with experiment. A full account of the work described in this section can be found in [31].

### 5. Neutrino nucleosynthesis of $^{138}\text{La}$ and $^{180}\text{Ta}$ and GT strength

Another example of the impact of GT strength distributions and its accurate description including configuration mixing on supernova nucleosynthesis is discussed below. A new calculation of neutrino nucleosynthesis predicts the charged-current reaction  $^{138}\text{Ba}(\nu_e, e^-)$  to be the origin of  $^{138}\text{La}$  (see also [32]) and, at least partly, also of  $^{180}\text{Ta}$  via the  $^{180}\text{Hf}(\nu_e, e^-)$  reaction [33]. While the present model represents a considerable improvement over the original approach [34], a large uncertainty in the quantitative estimates remains from the use of rather schematic RPA calculations to describe the response of the most important excitations, viz. GT and spin-dipole modes. Besides the need to introduce a quenching factor, a realistic description of the strength distributions requires the inclusion of complex configurations beyond the 1p-1h excitations considered in RPA. These correlations will fragment the GT strength more than described within RPA results and can in fact shift some strength over the relevant particle thresholds so that it will no longer contribute to the nucleosynthesis process. For example, excitation of GT transitions above the neutron threshold in  $^{138}\text{La}$  at 7.5 MeV excitation energy will produce  $^{137}\text{La}$  rather than  $^{138}\text{La}$ .

To study this problem, high-resolution measurements of the  $^{138}\text{Ba}(^3\text{He},t)$  and  $^{180}\text{Hf}(^3\text{He},t)$  reactions at zero degrees have been performed at RCNP, Osaka, using the same experimental techniques as described in the previous section. Details of the experiment can be found e.g. in [35]. The properties of the  $(^3\text{He},t)$  reaction at  $E = 140$  MeV/nucleon as a tool to measure

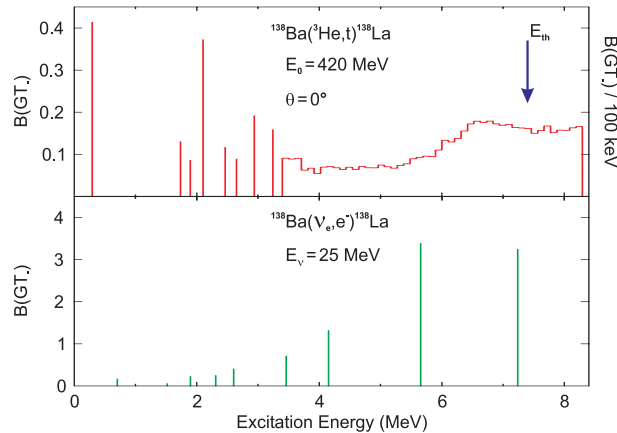


**Figure 6.** Top: Preliminary GT<sub>-</sub> strength distribution in  $^{138}\text{La}$  up to  $E_x = 10$  MeV deduced from the present experiment. Bottom: Theoretical GT<sub>-</sub> strength distribution used in the stellar evolution calculation calculations of [33]. The neutron threshold is denoted by  $E_{th}$ .

detailed GT distributions have been well established in recent years. A proportionality of the zero degree cross sections to the  $B(\text{GT})$  strength has been established by comparison with the GT strengths from the isospin-analogous  $\beta$  decays (see e.g. [36]).

Thus, for an extraction of absolute GT strengths a normalization to known weak GT decays is necessary. The accumulated data indicate [37] that this normalization is a smooth function of mass number  $A$ . The normalization is achieved for the case of  $^{138}\text{La}$  by a measurement of the g.s. transition populated in the  $(^3\text{He},t)$  reaction on the neighboring isotone  $^{140}\text{Ce}$ . Since the final nucleus  $^{140}\text{Pr}$  has a g.s.  $J^\pi$  value of  $1^+$ , the  $B(\text{GT})$  value of the well measured EC decay [38] from this nucleus can be used.

A preliminary  $B(\text{GT})_-$  strength distribution in  $^{138}\text{La}$  is presented in the top panel of Fig. 6. Up to  $E_x = 3.2$  MeV, individual transitions are resolved; above the strength is shown in 100 keV bins. The bottom panel shows the RPA results used in [33]. Clearly, the data exhibit much more fragmentation, particularly pronounced at excitation energies above 4 MeV. Furthermore, the total experimental  $B(\text{GT})_-$  strength below the neutron threshold is only about 70% of the calculated one. The astrophysical consequences are presently explored.

## 6. Concluding remarks

With these few selected examples I wanted to demonstrate that the study of the magnetic dipole and the related GT response in nuclei remains a field at the heart of nuclear structure physics. It is driven by a subtle interplay of single-particle and collective degrees of freedom and thus serves as an ideal testing of microscopic nuclear structure models including various degrees of configuration mixing. Furthermore, the properties of the GT resonance (and sometimes not only the gross features but also the fine structure) have a large impact on stellar dynamics and synthesis, in particular in supernova physics. Mandatory for future experimental research are taking advantage of the complementary information gained from electromagnetic and hadronic probes and the highest possible resolution.

## Acknowledgments

The experiments at RCNP have been performed in a Cape Town / Darmstadt / Johannesburg / Osaka collaboration and I thank all colleagues contributing to the realization of these experiments and their interpretation. I have benefitted in particular from numerous discussions



with and help from A. Byelikov, Y. Kalmykov, K. Langanke, P. von Neumann-Cosel, V.Yu. Ponomarev, A. Shevchenko and J. Wambach. Furthermore, I thank P. von Neumann-Cosel warmly for his great support in producing this manuscript. Finally, I am grateful to T. Otsuka and his colleagues for having invited me and for having created a very stimulating atmosphere at CDN05. This work has been supported by the DFG under contracts SFB 634 and 446 JAP 113/267/0-1.

## References

- [1] Arima A and Horie H 1954 *Prog. Theor. Phys.* **11** 509; **12** 623
- [2] Arima A, Shimizu K, Bentz W and Hyuga H 1987 *Adv. Nucl. Phys.* **18** 1
- [3] Bohle D et al 1984 *Phys. Lett.* **137** 27
- [4] Enders J, von Neumann-Cosel P, Rangacharyulu C and Richter A 2005 *Phys. Rev. C* **71** 014306
- [5] Ichimura M 1991 *Nucl. Phys. A* **522** 201c
- [6] <http://linaxa.ikp.physik.tu-darmstadt.de/richter/tokyo-2005.ppt>
- [7] Gaarde C 1985 *Proceedings Niels Bohr Centennial Conference on Nuclear Structure* Broglia R et al Eds (North-Holland, Amsterdam) 449
- [8] von Neumann-Cosel P, Poves A, Retamosa J and Richter A, 1998 *Phys. Lett. B* **443** 1
- [9] Laszewski R M, Alarcon R, Dale D S and Hoblit S D 1988 *Phys. Rev. Lett.* **61** 1710
- [10] Yako K et al 2005 *Phys. Lett. B* **615** 193
- [11] Steffen W et al 1983 *Nucl. Phys. A* **404** 413
- [12] von Neumann-Cosel P, Neumeyer F, Reitz B, Richter A, Wambach J 2000 *Phys. Rev. C* **62** 034307
- [13] Takayanagi K, Shimizu K and Arima A, 1988 *Nucl. Phys. A* **481** 313
- [14] Hix W R, Mezzacappa A, Bronson Messer O E and Bruenn S W, 2003 *J. Phys. G* **29** 2523
- [15] Langanke K and Martínez-Pinedo G, 2003 *Rev. Mod. Phys.* **75** 819
- [16] Auerbach L B et al 2001 *Phys. Rev. C* **64** 066501
- [17] Langanke K, Martínez-Pinedo G, von Neumann-Cosel P and Richter A, 2004 *Phys. Rev. Lett.* **93** 202501
- [18] Donnelly T W and Peccei R P 1979 *Phys. Rep.* **50** 1
- [19] Sober D I et al 1985 *Phys. Rev. C* **31** 2054
- [20] Poves A, Sánchez-Solano J, Caurier E and Nowacki F 2001 *Nucl. Phys. A* **694** 157
- [21] Honma M, Otsuka T, Brown B A and Mizusaki T, 2004 *Phys. Rev. C* **69** 034335
- [22] Caurier E et al 1999 *Phys. Rev. C* **59** 2033
- [23] Liebendörfer M et al 2004 *Astroph. J. Suppl.* **150** 263
- [24] Bergere R, 1977 *Lecture Notes in Physics* **61** 1
- [25] Diesener H et al 2001 *Nucl. Phys. A* **696** 292
- [26] Strauch S et al. 2000 *Phys. Rev. Lett.* **85** 2913
- [27] Shevchenko A et al 2004 *Phys. Rev. Lett.* **93** 122501
- [28] Fujita Y 2005 contribution to these proceedings
- [29] Wakasa T et al 2002 *Nucl. Instrum. Meth. A* **482** 79
- [30] Coifman R Ed. 1992 *Wavelets and Their Applications* (Jones and Barlett, Boston)
- [31] Kalmykov Y et al 2005 *Phys. Rev. Lett.* submitted
- [32] Goriely S, Arnould M, Barzov I and Rayet M 2001 *Astron. Astrophys.* **375** L35
- [33] Heger A et al 2005 *Phys. Lett. B* **606** 258
- [34] Woosley S E, Hartmann D H, Hoffman R D and Haxton W C, 1990 *Astroph. J.* **356** 272
- [35] von Neumann-Cosel P 2005 *Prog. Part. Nucl. Phys.* **55** 397
- [36] Fujita Y et al 1999 *Phys. Rev. C* **59** 90
- [37] Fujita Y 2005 private communication
- [38] Peker L K 1994 *Nucl. Data Sheets* **73** 261